From cubic palladium to concave core-shell platinum palladium nanoparticles: Evolution of the structure and their electrochemical properties

Tymen, S.; Scheinost, A. C.; Lozano Rodriguez, M. J.; Friebe, C.; Schubert, U. S.;

Originally published:

February 2018

Journal of the Electrochemical Society 165(2018)3, H67-H77

DOI: https://doi.org/10.1149/2.0021803jes

From cubic palladium to concave core-shell platinum palladium nanoparticles: Evolution of the structure and their electrochemical properties

Simon Tymen[1], Andreas C. Scheinost[2, 3], Christian Friebe[1, 4], Ulrich S. Schubert[1, 4, 5]

[1] *Laboratory of Organic and Macromolecular Chemistry (IOMC), Friedrich-Schiller University Jena, Philosophenweg 7, 07743 Jena, Germany*

[2] *The Rossendorf Beamline, European Synchrotron Radiation Facility (ESRF), 38043 Grenoble, France*

[3] *Molecular Structure Division, Institute of Radiochemistry Forschungszentrum Dresden-Rossendorf (FZD), Dresden, Germany*

[4] *Center for Energy and Environmental Chemistry Jena (CEEC Jena), Friedrich Schiller University Jena, Philosophenweg 7a, 07743 Jena, Germany*

[5] *Jena Center for Soft Matter (JCSM), Friedrich-Schiller University Jena, Humboldtstraße 10, 07743 Jena, Germany*

Abstract

Pt-Pd nanoparticles, from pure Pd nanocubes to Pd-Pt core-shell nanoparticles, are synthesized following different methods and intensively investigated, in view of a potential application in fuel cells, as catalysts for the oxygen reduction reaction (ORR). The galvanic replacement is an attractive method to prepare bimetallic particles with high catalytic activity and a high control of the size, shape and chemical composition of the particles, varying with the experimental conditions during the synthesis. The influence of the time with the transformation from pure Pd nanocubes to concave core-shell Pt-Pd nanoparticles synthesized by galvanic replacement (with a Pd core and a mix of Pt and Pd in the surface) is examined: after different times of preparation, the morphology of the particles was monitored by Transmission Electronic Microscopy (TEM) coupled with Energy Dispersive X-Ray Spectroscopy (EDS) for the chemical composition. Via X-Ray diffraction spectroscopy (XRD), the crystallographic structure and the variation of size, lattice parameters, *d*-spacing, and composition were determined. The Extended X-ray Fine Structure (EXAFS) measurements show the formation of a Pt-Pd alloy at the surface of the particles for all samples. Finally, the electrochemical determination of the catalytic activity and stability tests revealed two different particle types as candidates to replace pure Pt as catalyst in the Proton Exchange Membrane Fuel Cells (PEMFC) due to their enhanced stability, higher catalytic activity, and lower Pt content.

Keywords: Platinum, palladium, nanoparticles, oxygen reduction reaction, EXAFS

Introduction

Today the problems of climate change and the environmental pollution necessitate the replacement of fossil fuels by means of new energy sources and sustainable technologies. In this regard, proton exchange membrane fuel cells (PEFMCs) with their high efficiencies at ambient temperature represent highly promising alternatives. One of the main chemical reactions in PEFMCs, the oxygen reduction reaction (ORR) depends strongly on the usage of suitable catalysts and, thus, many researchers are working on the development of new materials with a higher catalytic activity for the ORR. Unfortunately, most of the catalysts are based on platinum, a transition metal that does not occur abundantly and is, hence, too expensive for a large scale utilization. Different approaches are tested aiming at the reduction of the cost of the cells and the improvement of their performances. The diminution of the amount of platinum via bimetallic catalysts (core-shell, alloys...) chatenet$_{s}ilver-platinum_{2}003,,ocampo_{c}haracterization_{2}006andnanostructuredmaterialswithdifferentshapesandsizesofpa$
$shellnanoparticles(NPs),wefollowedtheevolutionofthestructureviaTEM-EDSobservationsandEXAFSm$
$Levichanalysis,theelectrochemicalpropertiesoftheparticles(catalyticactivity,kinetic,stability)werecompare$
$shellPd-Ptnanoparticlescouldbepreparedbygalvanicreplacement.Furthermore,in\text{-}situXAFSmeasurements$
$transformedEXAFSspectra,weobservedanevolutionoftheparticles(withandwithoutoxide).WiththeIterativ$

Experimental section

Synthesis of Pt-Pd nanoparticles

Depending on the particles type, size, shape, and composition, different methods were used to synthesize Pd-Pt nanoparticles (NPs) in aqueous or organic solution huang$_{s}ynthesis_{2}012,,hong_{c}ontrolled_{2}012,c$
$shellnanoparticleszhang_{p}dpt_{2}010orPd-Ptalloynanocages,zhang_{f}acile_{2}011thehexachloroplatinicacid(H_2PtC$
$Firstlythesynthesisofcubic Pdnanoparticles,followedbypreparationofthePt-Pdcore-shellnanoparticles.$
The synthesis of the Pd NPs was performed in aqueous solution: 0.6 g of ascorbic acid (AA, Sigma Aldrich, 98%), 3 g of potassium bromide (KBr, Sigma Aldrich, 99%), 1.85 g of potassium chloride (KCl Sigma Aldrich, 99%), and 1.05 g of poly(vinylpyrrolidone) (PVP, Alfa Aesar, 98%) were added to 80 mL of distilled water. The solution was sonicated for 2 min and heated to 80 °C. After 10 min, 30 mL of sodium tetrachloropalladate (6.5×10^{-2} mol.L^{-1}, Na_2PtCl_4, Sigma Aldrich, 98%) were added with a syringe (1 mL.min^{-1}). Afterward, the solution was maintained at 80 °C under magnetic stirring for 3.5 h. The Pt-Pd NPs were prepared in a second step: 10 mL of the solution containing Pd nanoparticles were mixed with 70 mL of an aqueous solution composed of 3 g of KBr and 0.333 g of PVP. The solution was heated to 90 °C and 30 mL of K_2PtCl_4 (3×10^{-3} mol.L^{-1}, Sigma Aldrich, 98%) were added (1 mL.min^{-1}) under magnetic stirring. Different times of synthesis were used to study the evolution of the particles: 0.6 h, 2 h, 4 h, 6 h, 8 h, and 17 h. After the synthesis, the particles, collected by centrifugation were washed and rinsed several times with water and ethanol. Afterwards, the solution containing clean particles was dried in the oven at 70 °C.

Coating the particles on carbon powder

For a sample, composed of 40% particles and 60% of carbon, 40 mg of particles were added to 25 mL of ethylene glycol (VWR), and the mixture was sonicated for 15 min. A mixture of 60 mg of Vulcan XC-72R carbon powder in 25 mL of ethylene glycol at pH 2 (adjusted with nitric acid solution, 2 mol.L^{-1}, Sigma Aldrich, 70%, purified by re-distillation) was sonicated for 30 min. After sonication, both mixtures were merged, sonicated for 1 h and stirred for one night with a magnetic stirrer. Afterwards, the mixture was heated to 40 °C and filtrated. The resulting

particles were collected by microfiltration and dried for 5 h at 70 °C in an oven. The method was used analogously for all particles.

TEM-EDS characterization

The nanoparticles were characterized with a high-resolution transmission electron microscope (HR-TEM) JEOL JEM-3010 operating at 300 keV and equipped with an X-Ray analyzer Oxford. Before the experiments, the aqueous solution containing the nanoparticles was homogenized by sonication and dispersed on a TEM grid (copper covered by a carbon film). The sample was subsequently dried under vacuum before the introduction in the main chamber of the TEM.

EXAFS measurements

The Pt-L_{III} edge and Pd-K edge EXAFS measurements were performed at the Rossendorf Beamline (BM20A) at the European Synchrotron X-Ray Facility (ESRF, Grenoble, France). The synchrotron beam was monochromatized using a water-cooled Si(111) double-crystal monochromator (DCM). A first, 1.4-m long, Pt-coated, meridionally bent Si mirror was used before the DCM for collimation, and a second, 1.3-m long, Pt-coated, toroidal Si mirror after the DCM was used for vertical and horizontal focusing. The rejection of higher harmonics of the complete setup is better than 104. The measurements were done at room temperature, either in transmission or fluorescence mode, using ionization chambers and a 13-element high-purity Ge detector (Canberra) with a digital spectrometer (XIA X-Map). Before measurements, the particles coated on carbon (40 % particles) were compressed to form pellets (1 g) with addition of boron nitride powder (BN, Sigma Aldrich, 98%) for a better stability. Energy calibration, averaging of several scans, and dead-time correction of fluorescence signals were done with the software SixPackwebb$_{s}ixpack_{2}$005.$Subsequentdatareductionstepswereperformedwiththe WinXAS software.ressler_{w}i$ $orderpolynomialfunctionfittedthroughthepre-edgeregion, andasecondorderpolynomialfunctionfittedthrou$ $edgeregion.Spectrawerethenconvertedfromenergyintophotoelectronskineticenergyunits(k-space)byarbitrar$ $edgeregionusingtheauto-splinealgorithmofWinXAS.Thesuch-obtainedEXAFSfunctionswere$ k^3-weighted and then Fourier-transformed to R space using a Bessel window function across a k range of 2 to 15 Å^{-1}. Theoretical phase shift and amplitude functions for the shell fits were calculated with FEFF 8.2ankudinov$_{r}elativistic_{1}$997$basedonPt, Pt-Pd, andPdmetalclusterswithaface-$ $centeredcubic(fcc)crystallographicstructure.Theshellfitwasthenperformedwith WinXAS toderivecoordinati$ $Wallerfactors$(σ^2), and phase shift correction (ΔE_0).

X-Ray Diffraction (XRD)

The X-Ray Diffraction (XRD) experiments were performed using a Rigaku Miniflex600 diffractometer equipped with an energy dispersive D/teX Ultra silicon strip detector. For XRD measures, Cu $K_{\alpha 1}$ radiation (wavelength:1.54184 Å) was used at 40 kV and 15 mA. The scanning range (2θ) was from 30 to 90 ° with a scan rate of 1°.min^{-1} and an interval of 0.02 °. Before characterization, about 30 mg of catalyst powder was pressed to obtain a homogeneous distribution in the sample holder. The Rietveld analysis was done based on Pt, Pd, and Pd-Pt with *fcc* structures coming from the Crystal Open Database (COD)grazulis$_{c}rystallography_{2}$012$withthesoftwareMAUDl.lut$

Electrochemical measurements

For all the measurements, a potentiostat (Princeton Applied Research VersaStat MC) with a standard three electrodes configuration was used with a glassy carbon rotational disc electrode (RDE, Princeton Applied Research, model 636A, geometric area of 0.1963 cm^2) as the working electrode, a Hg/Hg_2SO_4 as the reference electrode, and a platinum wire as counter electrode. The electrochemical studies were carried out in 70 mL of $HClO_4$, (1× 10^{-1} mol. L^{-1}) electrolytic

solution made from 18 MΩ microfiltrated water. Before experiments, the RDE was polished and rinsed with high purity water. All potentials are given versus the Standard Hydrogen Electrode (SHE).
The different nanoparticles were characterized in the form of an ink made by dissolution of 9 mg of PtPd/C catalyst powder in a mixture of 0.25 mL of water and 2.25 mL of isopropyl alcohol (IPA, Merck, 99.5%). After 15 min of sonication, 12 µL of the ink are deposited on the RDE glassy carbon support (3 × 4 µL) and the film was protected by the deposition of 7 µL of Nafion® (perfluorinated resin solution, 5 wt.%, Sigma Aldrich) diluted in methanol (1:100). After deposition, the fresh film was electrochemically cleaned by cyclic voltammetry (60 cycles) in a range from 0.050 to 1.200 V at 0.100 $V.s^{-1}$. The determination ECSA was done with the same method in the same potential range at a scan rate of 0.020 $V.s^{-1}$ with the electrolyte saturated with N_2. After the ECSA determination, the oxygen reduction reaction (ORR) test and the electrochemical impedance spectroscopy (EIS) experiments were conducted in an $HClO_4$ (0.1 M) O_2-saturated solution. The EIS was measured at a dc potential of 0.5 V, applying ac frequencies from 1×10^5 to 5×10^{-2} Hz and an ac amplitude of 0.010 V as well as an RDE rotation velocity of 1600 rpm. The catalytic activity was calculated after measurements by linear scan voltammetry (LSV) within a potential range from 0.3 to 1.2 V under rotation (1600 rpm) at 0.005 $V.s^{-1}$. All electrochemical experiments were done at ambient temperature (25 °C).

Results and discussion

Characterization of the Pt-Pd nanoparticles by TEM and EDS

The Pt-Pd nanoparticles were prepared using the galvanic replacement method and the evolution of their structure was studied after different times of synthesis. The TEM-EDS investigations permitted the analysis of the structure of the NPs (size, shape, repartition and composition) without modification of the samples (the particles were directly deposited on a TEM grid). The TEM observations revealed a progressive evolution of the NPs with the time of synthesis (Figure 1), with a particle size of around 20 nm for all the samples.

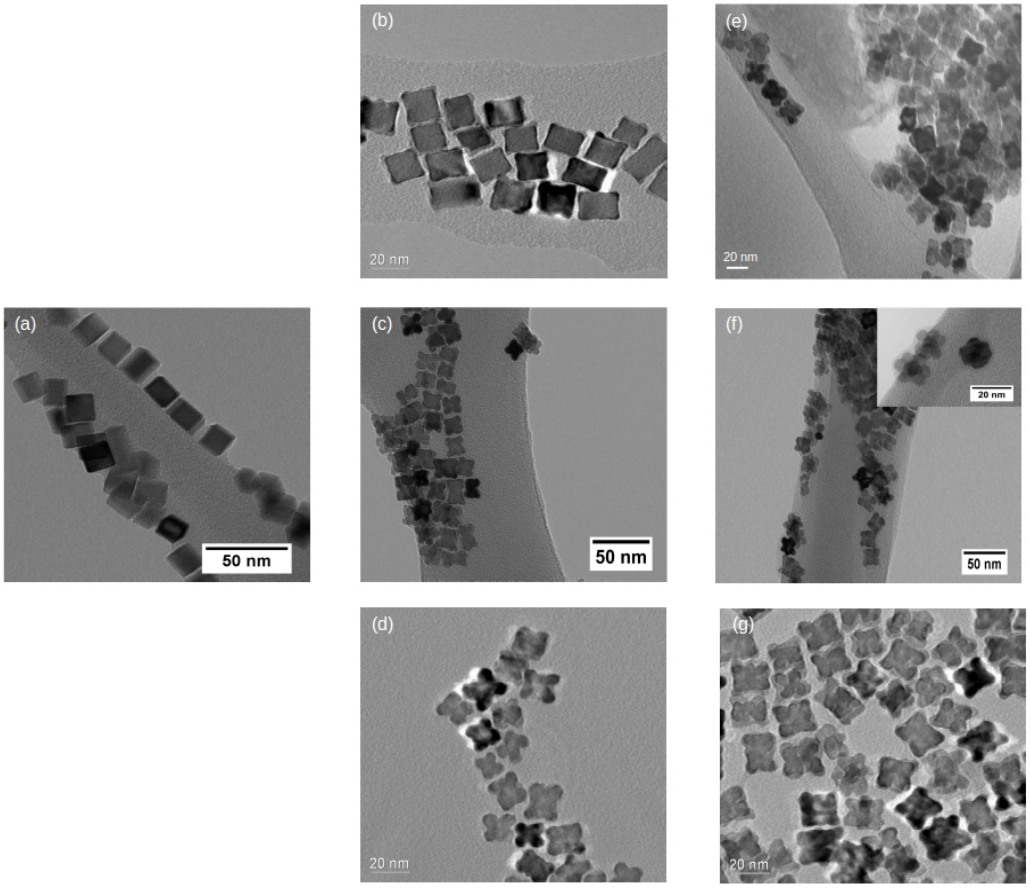

Figure 1: *Evolution of the nanoparticles structure followed by TEM after different times of synthesis. (a) Pure Pd nanocubes, (b) Pt-Pd 0.6 h ,(c) Pt-Pd 2 h, (d) Pt-Pd 4 h, (e) Pt-Pd 6 h, (f) Pt-Pd 8 h and (g) Pt-Pt 17 h.*

The core of the particles, constituted of Pd, is darker due to the smaller atomic number of Pd (Z=46) compared to Pt (Z=78). Before the galvanic replacement and the addition of Pt, pure Pd NPs with a well-defined cubic shape and an average size of 18 nm (without aggregates) were visible on TEM pictures. Through the addition of a Pt solution, the formation of PtPd NPs began via galvanic replacement and co-deposition of Pt.
For the particles prepared within 0.6 h, a thin layer of Pt (confirmed by EDS) appeared on the surface of the particles. The Pt film formation started at the corners of the Pd cubes and the thickness of the Pt shell increased to form a layer of Pt over the Pd core.
The concavity of the NPs and the thickness of Pt layer increased with the time of synthesis. After 4 h, a concave Pd core became apparent. There were no significant variations of the size of the particles with the time of synthesis. No aggregates were visible and the shape of the particles was homogeneous (excepted for some samples where some core-shell nanoparticles with a flower structure were visible after 6 h and 8 h of synthesis). After the characterization of the particles via TEM, the EDS confirmed that the particles are composed of Pt, Pd and small quantities of Br. The presence of bromine in the spectra was due to an incomplete galvanic replacement, i.e. the bromide was not completely replaced by the Pt. An evolution of the amounts of Pt and Pd with the time of synthesis was observable (Table 1): The ratio of Pt increased until 4 h and

decreased for the particles synthesized in 6 h, with 22 wt. % of Pt. After 8 h, there was again an increase (26 wt. % of Pt) and, finally, for the particles synthesized in 17 h, the ratio of Pt was equivalent to the 4 h particles (35 wt. %).

XRD analysis

On the XRD spectra (Figure 2), the main characteristic peaks of the *fcc* Pt and Pd crystals, corresponding to the planes (111), (200), (220) and (311), are visible, confirming an *fcc* crystalline structure composed of Pd and Pt atoms for all the particles. XRD patterns for the different particles are similar, which denotes analogous bulk compositions and no peaks that correspond to Pt or Pd oxides are observable.

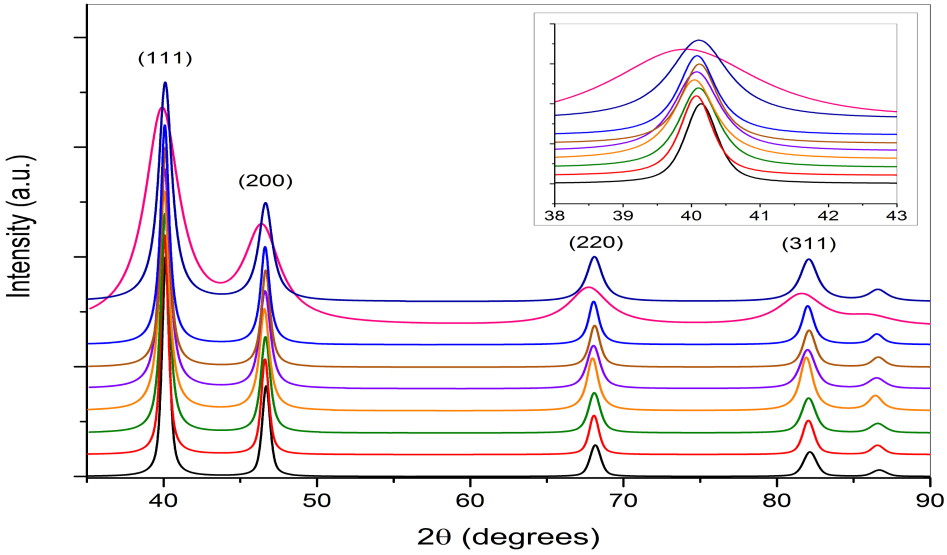

Figure 2: *Shift-corrected and normalized XRD spectra with the Miller indices of the different catalysts. Inset: Magnification of the (111) peak.*

After the normalization of the spectra with respect to the intensity of the well-defined (111)-based peak, the inter-planar distances d were calculated using the Bragg's law:

$$2.\mathrm{d}.\sin(\theta) = n.\lambda \tag{1}$$

where n is the integer factor, θ is the Bragg's angle (degrees), and λ is the wavelength of the X-rays, (Cu $K_{\alpha 1}$ radiation, 1.54184 Å).
The average size of the particles, τ, was calculated from the widths of the (220) diffraction peaks on the spectra via Scherrer's equation, which is valid for nanometric objects:

$$\tau = \frac{\mathrm{K}.\lambda}{\beta.\cos(\theta)} \tag{2}$$

where K is a shape factor (between 0.9 and 1.0, here 0.94) considering an *fcc* isotropic structure, λ is the wavelength of the X-rays, β (radians) the FWMH, and θ the Bragg's angle (degrees) of the peak that was selected to calculate the particles size.

To obtain an estimation of the quantity of Pt and Pd in the particles and to compare these values to the results coming from the EDS measurements, the Vegard's law was applied. dutta$_{s}ignificant_{2}013This was_{p}$ $So, the composition of the mixture is approximately determined by the equation$:

$$\mathrm{a}_{Pt(1-x)Pdx} = (1-x).\mathrm{a}_{Pt} + x.\mathrm{a}_{Pd} \tag{3}$$

with x as the molar fraction of Pd in the particles. The lattice parameters of the solid solution $a_{(Pt(1-x)Pdx)}$, were measured by XRD, and the theoretical values of the lattice parameters of Pt, (a_{Pt}), and Pd, (a_{Pd}), were the theoretical values for Pt and Pd with a *fcc* structure coming from the C.O.D grazulis$_{c}rystallography_{2}012, 3.923and3.891, respectively.$
After the analysis of the spectra, the evolution of the lattice parameters for the different samples was studied (Table 1).

Table 1: *Summary of the results from the XRD measurements and composition of the particles measured by EDS.*

Sample	**Lattice parameter (Å)**	***d-spacing* (Å)**	**Particle size (nm)**	**Pd molar fraction (%) (XRD), error: $\simeq 10\%$**	**Pd weight (wt.%) (error, %) (EDS)**	**Pt weight (wt.%) (error, %) (EDS)**	**Pd molar fraction (%) (EDS)**
Pd nanocubes	3.891	2.2468	19.24	100	100	0	100
Pt-Pd 0.6 h	3.892	2.2471	20.03	94	91 (3)	9 (10)	95.9
Pt-Pd 2 h	3.894	2.2482	15.53	88	81 (8)	19 (6)	87.2
Pt-Pd 4 h	3.900	2.2517	14.39	70	65 (7)	35 (11)	70.5
Pt-Pd 6 h	3.897	2.2496	13.43	78	78 (8)	22 (7)	80.5
Pt-Pd 8 h	3.893	2.2479	16.74	91	74 (8)	26 (8)	80.4
Pt-Pd 17 h	3.896	2.2498	16.06	82	65 (8)	35 (11)	71

For the commercial Pt and Pd spectra, the same diffraction profile as for a standard material appears, with lattice parameters of 3.894 Å for the Pd and 3.913 Å for the Pt, which deviate negligibly from the theoretical ones due to inhomogeneities. For the particles, the lattice parameters and the *d-spacing* (interatomic distance between plane on the crystal) are between those of pure Pd and pure Pt. The lattice parameters and *d-spacing* values evolved in accordance with the ratio of Pt in the particles (measured by EDS): the Pt-rich particles feature higher lattice parameters and *d-spacing* values, corresponding to the expansion of the crystalline structure with the replacement of Pd atoms by Pt. The different sizes of particles found by application of Scherrer´s equation (Eq. 2) were comparable to the sizes estimated from the TEM pictures. With progressing synthesis times, the particle size decreased from 20 nm for the Pd nanocubes

and the Pd-Pt 0.6 h core-shell nanoparticles to 13.4 nm after 6 h. For longer times, the size increased again to about 16 nm.
The first step of the evolution of the chemical composition of the particles, determined using Vegard's law and the weight fraction measured by EDS, was similar. An increasing Pt ratio for 4 h (35 wt % Pt), followed by a diminution of the Pt content after 6 h. Afterwards, XRD experimental results indicate a further decreasing Pt content (8 h), which rises again for the 17 h samples. In contrast, according to EDS, the Pt content is continuously increasing from 6 h to 17 h. These differences probably come from derivations of the law, which were already observed by other researchers working on alloys $\mathrm{kuo}_v egards_2 004, , lubarda_e ffective_2 003$.

EXAFS measurements

The EXAFS measurements at Pt-L_{III} for the different PtPd nanoparticles coated on carbon were compared to pure Pt foil, to see the differences between pure Pt and the particles. The Fourier-transformed spectra are presented in Figure 3. The data collected at the Pt-L_{III} edge showed a well-defined double peak between 2 and 3 Å (uncorrected for phase shift) for all the nanoparticles. The FEFF modeling using clusters with different ratios of Pd and Pt revealed that this double peak arises from the presence of both Pt and Pd neighbors in a (nearly) equal proportion within the first shell. By comparison, the commercial Pt showed only one peak as expected from the exclusive presence of Pt neighbors.

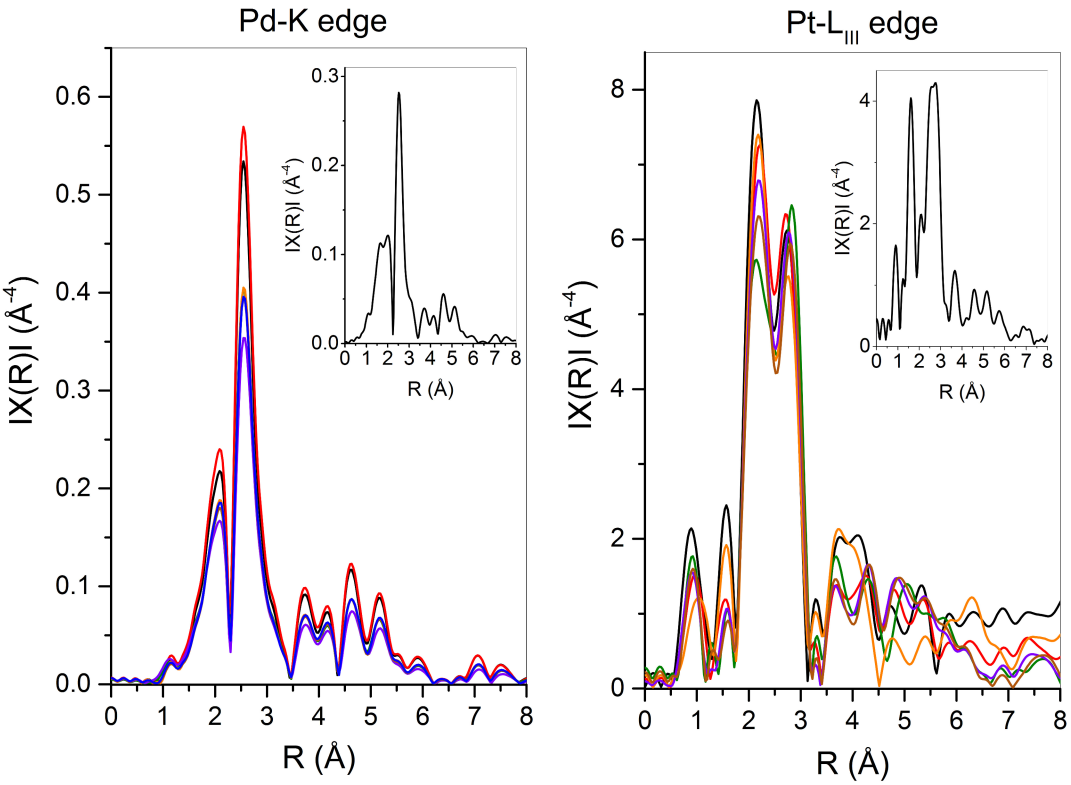

Figure 3: *Fourier-transformed EXAFS spectra of the nanoparticles. Pure Pd or Pt (black), 0.6 h (red), 2 h (green), 4 h (orange), 6 h (violet), 8 h (brown), 17 h (blue) at Pd-K (left) and Pt-L_{III} edges (right).*

At the Pd-K edge, the main strong peak in the Fourier-transformed spectra at $R \sim 2.74$ suggests the predominance of only one type of neighbors (Figure 3), most likely the Pd, which was confirmed by the shell fit of the data (Table 2 and 3). As shown by the Pt-Pt and Pt-Pd data, Pt is surrounded by both Pt and Pd neighbors at distances of 2.72 to 2.74 Å, which is in line with the crystallographic value of 2.74 Å.toshima$_b$*imetallic*$_1$998*ThesumofbothPt* − *PtandPt* − *PdCNsiscloseto*12, *consideringtherelativelyhigherrorof* $\sim$ 25 %, and the Pd:Pt ratio is slightly above 1. Relatively small Debye-Waller factors indicate a small static and vibrational disorder. All these results are in line with the *fcc* structure (also validated by XRD), where the Pt resides in a local structure surrounded by Pd and Pt atoms.

Table 2: *Coordination numbers (CN), interatomic distances R, Debye Waller factors (σ^2), and energy shifts (ΔE_0) at the Pt-L_{III} edge.*

Pt-L_{III} edge								
Sample	**Pt-Pt shell**			**Pt-Pd shell**			**ΔE_0**	**$R_{factor}{}^2$**
	CN	**R [Å]**	**σ^2 [Å^2]**	**CN**	**R [Å]**	**σ^2 [Å^2]**	**[eV]**	**res (%)**
Pt-Pd 0.6 h	6.7	2.72	0.0058	4.8	2.72	0.0058	5.9	5.4
Pt-Pd 2 h	6.2	2.73	0.0057	5.1	2.73	0.0057	7.1	4.0
Pt-Pd 4 h	8.7	2.75	0.0055	3.5	2.74	0.0055	8.3	2.3
Pt-Pd 6 h	6.7	2.74	0.0061	4.8	2.74	0.0061	7.8	3.3
Pt-Pd 8 h	7.3	2.74	0.0056	4.8	2.74	0.0056	7.7	2.2
Pt-Pd 17 h	7.6	2.74	0.0056	4.3	2.74	0.0056	7.8	2.7

For the data at the Pd-K edge (Table 3), the Pd-Pd distance of the nanoparticles as well as for the Pd reference is also 2.74 Å, as expected for the *fcc* structure.Zhang2011a In contrast, the Pd-Pt bond length of 2.71 Å was slightly but significantly smaller than the bond length measured for the Pd-Pd pairs.

Table 3*: Coordination numbers (CN), interatomic distances R, Debye Waller factors (σ^2), and energy shifts (ΔE_0) at the Pd-K edge.*

Pd-K edge								
Sample	**Pd-Pt shell**			**Pd-Pd shell**			**ΔE_0**	**$R_{factor}{}^2$**
	CN	**R [Å]**	**σ^2 [Å^2]**	**CN**	**R [Å]**	**σ^2 [Å^2]**	**[eV]**	**res (%)**
Pt-Pd 0.6 h	0.6	2.71	0.0051	11.2	2.74	0.0009	9.1	0.3
Pt-Pd 2 h	1.4	2.71	0.0054	10.7	2.74	0.0054	5.4	1.6
Pt-Pd 4 h	1.7	2.71	0.0053	10.5	2.74	0.0053	5.6	1.7
Pt-Pd 6 h	1.7	2.72	0.0053	9.5	2.74	0.0056	8.7	4.2
Pt-Pd 8 h	1.7	2.70	0.0053	10.2	2.74	0.0053	5.1	1.3
Pt-Pd 17 h	1.8	2.71	0.0052	10.2	2.74	0.0052	5.3	1.5

In contrast to the Pt values, the Pd-K edge based CNs suggested that the Pd is prevalently surrounded by other Pd atoms (CNs between 9.5 and 11.2) and only by a smaller number of Pt atoms (CNs between 0.6 and 1.8); the variation of CNs among the different samples was not statistically significant.

The results of the analysis of the EXAFS spectra from both the Pd-K and Pt-L_{III} edges can be explained with a well-structured Pd metal core where most of the Pd atoms possess Pd neighbors and that is surrounded by a thin Pt shell with most of the Pt atoms having Pd neighbors. Confirming the TEM and EDS observations, the higher coordination numbers for the Pt-Pt bond from the Pt-L_{III} measurements (Table 2) suggest an aggregation of Pt in the surface, with a little increase after 8 and 17 hours of synthesis.

Electrochemical properties

Electrochemically active surface area (ECSA)

The ECSA was calculated using the charge transferred during the hydrogen adsorption/desorption on the surface of the electrode (Q_H) and the mass (m) of deposited catalyst PtPd/C. These chemical processes appear on the voltammograms between 0.05 and 0.30 V (Figure 4). Q_H was calculated by integration of the area under the CV curve (Eq. 4). The ECSA was determined following Eq. 5, considering a reference charge density for the oxidation of a monolayer of hydrogen of 2.4×10^{-4} C.cm^{-2} for the pure Pd and 2.1×10^{-4} C.cm^{-2} for the pure Pt and PtPd nanoparticles. The roughness factor mayrhofer$_{m}easurement_{2}008(Eq.6)permitsthecomparisonoftheactivesurfacearea(A_{real})$

$$\mathrm{Q}_H = \frac{\int idE}{\nu} \tag{4}$$

where$i$ is the current, E is the potential, and ν is the scan rate.

$$\mathrm{ECSA} = \frac{1}{2,1 \times 10^{-4}\mathrm{C.\ cm^{-2}}} \times \frac{Q_H}{m_{PtPd}} \tag{5}$$

$$\mathrm{r}_f = \frac{A_{real}}{A_{geometric}} \text{ with } A_{real} = \frac{Q_H}{2,1 \times 10^{-4}\mathrm{C.\ cm^{-2}}} \tag{6}$$

All ECSA and roughness factor values possess an estimated error of more than 10 % with three samples per particle batch. The total error included the experimental error (the reference electrode, the shift of the potential, the homogeneity of the deposition on the electrode) and the mathematical error of the charge calculation by integration. The ECSA values are in the same range like the literature values for Pt-Pd NPs on carbon zhou$_{d}urability_{2}010$.
For all CVs (Figure 4), three characteristic regions are visible on the voltammograms: Firstly, the hydrogen adsorption-desorption occurs between 0.05 and 0.30 V, with the adsorption of hydrogen from 0.05 to 0.075 V and the desorption until 0.30 V. Subsequently, the double layer charging (0.30 to 0.65 V), and, between 0.65 and 1.20 V, the formation and adsorption of hydroxide anions and oxygen on the catalyst followed by their reduction take place (Figure 4). The ECSA for the 4 h Pt-Pd nanoparticles (100.6 m^2. g^{-1}), is higher than for the commercial Pt coated on carbon (84.04 m^2. g^{-1}), while the ECSA of the particles synthesized in 2 h is similar. A significant increase of the ECSA between pure Pd and PdPt core-shell nanoparticles is apparent, with high ECSA values for the particles (Table 4) with a concave shape and a thin layer of Pt-Pd visible on the TEM images (cf. Figure 1). For the particles with a longer synthesis time (6 and 8 h), the ECSA decreases, with values lower than the pure Pd nanocubes. After 17 h, the ECSA is higher than for pure Pd nanoparticles again and in the same range like the particles that had been synthesized in less than 4 h.
The higher ECSA values for the core-shell Pt-Pd NPs (except for the particles synthesized within 6 and 8 h) compared to the pure Pd nanocubes are caused by different factors.

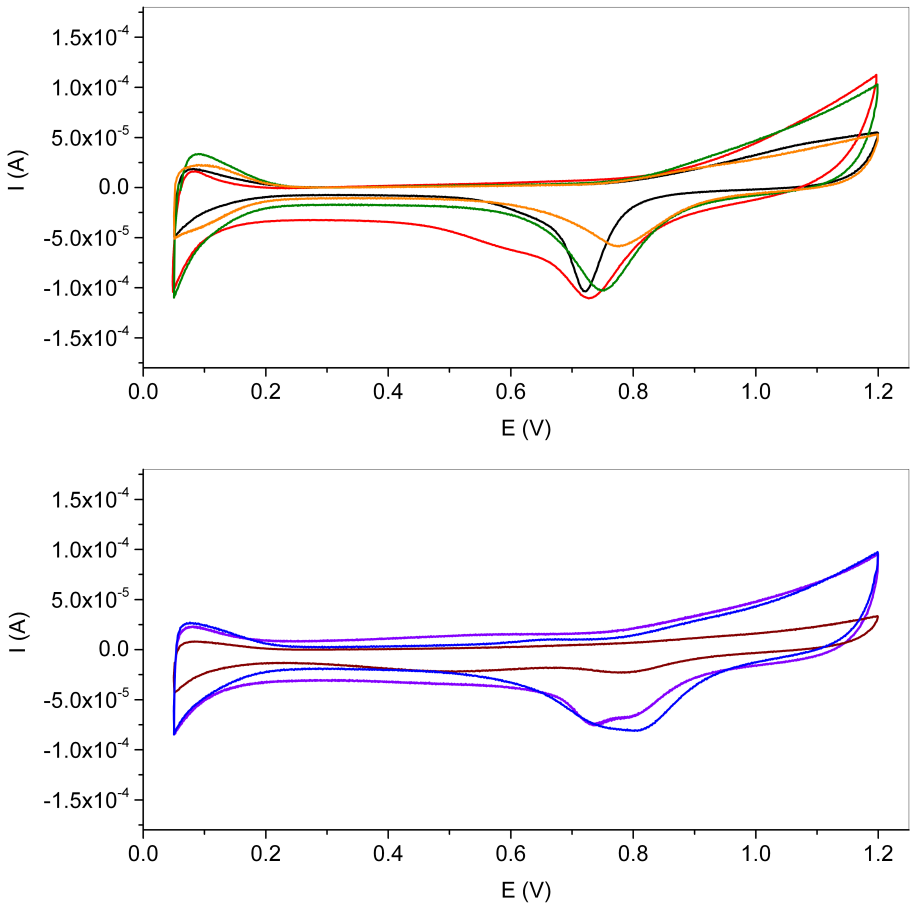

Figure 4: *ECSA typical voltammograms: Pure Pd (black), 0.6 h (red), 2 h (green), 4 h (orange), 6 h (violet), 8 h (brown), 17 h (blue).*

Using the galvanic replacement, the formation of a thin Pt or Pt-Pd layer on the surface of the Pd core occurs, which is visible in the TEM images and confirmed by the EDS measurements. The Pt shell thickness is a main parameter to control the activity of core-shell catalysts[17]. Furthermore, the geometric and electronic structure of the core is also important for the catalytic performances.
With the development of concave nanoparticles, the structure changes significantly and important modifications of the particle shape and the thickness of the shell occur. The co-deposition of Pt and the replacement of bromine atoms during the galvanic replacement, with the formation of a Pt-Pd alloy (cf. EXAFS results) with a different electronic structure, leads to additional chemical active sites jebaraj$_o$$xygen_2$016, $whichmayalsocauseahigherECSAvalue.Inaddition, thePt$: $Pdratiowithintheparticleshasagreatinfluenceon theECSAandtheORRperformanceszhang_aqueous - phase$; $Pdalloythatisformedintheshelloftheparticles(detectedbyEXAFS)changes, withanevolutionofthecrystallin$
The evolution of the shape of the particles, from pure Pd nanocubes to concave core-shell concave nanocubes and the different Pt:Pd ratios with the time of synthesis also contribute to new chemical properties. A quantification by ICP-MS, and XPS measurements is necessary to gain more information, in particular via the detection of very small concentrations and their distribution on the surface of the particles.

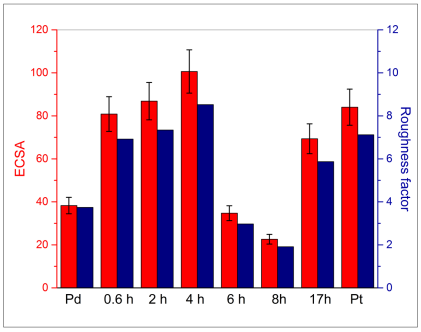

Figure 5: *Electrochemically active surface area (red) with errors (black) and roughness factors (blue) for the different samples.*

Oxygen reduction reaction

The ORR kinetics were studied applying the Koutecký-Levich equation on the parameters extracted from the voltammetric experiments. The electrical current (i), measured by licyclic voltammetry, was transformed into the current density j using the geometric area of the electrode (0.1963 cm^2). Three different regions are apparent on the voltammograms: Until 0.60 V, the reaction on the surface of the electrode is controlled by diffusion processes (the mass transport). When the potential increases, between 0.60 and 0.85 V, diffusional and kinetic processes occur on the surface of the electrode with adsorption and desorption of oxygen atoms and OH radicals, and a possible formation of H_2O_2. Finally, up to 0.85 V, the dominant processes are pure kinetic phenomena.

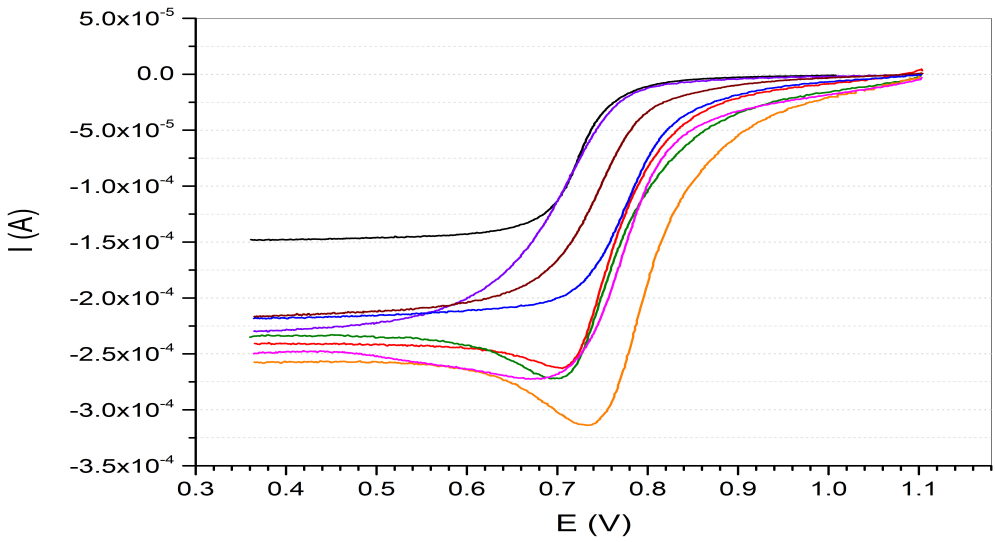

Figure 6: *Characteristic voltammograms for the ORR of NPs: Pd (black), 0.6 h (red), 2 h (green), 4 h (orange), 6 h (violet), 8 h (brown), 17 h (blue) in aqueous $HClO_4$ saturated with O_2 (5 $mV.s^{-1}$, 1600 rpm).*

On the voltammograms (Figure 6), the onset of the ORR for the pure Pd is found at 0.75 V. For

the different Pt-Pd NPs and the pure Pt sample, the onset potential increases gradually until 0.87 V. Working with a RDE at 1600 rpm ensures fast convective transport of the active species. The catalytic activities of the particles were compared via the mass activity j_{mass}, defined as the kinetic current density j_k, normalized to the mass of catalyst that is deposited on the surface of the electrode m_{PtPd}. The current density j from the measurement using an RDE at 1600 rpm is composed of the kinetic current density j_k and the Levich current density j_L by the Koutecký-Levich equation:

$$\frac{1}{j} = \frac{1}{j_L} + \frac{1}{j_k} \tag{7}$$

The kinetic current density j_k is calculated with the values of the current densities j at 0.85 V and j_L at 0.50 V for the anodic scan.
The received kinetic current density at 0.85 V was normalized to the mass of catalyst m_{PtPd} to compare the catalytic performances of the particles for the ORR:

$$j_{mass} = \frac{j_k}{m_{PtPd}} \tag{8}$$

For the different samples, the ORR mass activities were determined (Table 4) whereas the Pd nanocubes show the lowest mass activity (7.6 A.g^{-1}) due to the absence of Pt. It is known from literature that Pd possesses a significantly lower catalytic activity for the oxygen reduction reaction in acid media than Pt or bimetallic NPs based on Pd (alloys savadogo$_n$$ew_2$004$orcore-shellstructuresgupta_electrochemical_2$014, , $golikand_study_2$011).$Theadditionofanothermetalbele_highly_2$014, , I

Table 4: *Catalytic properties and their evolution for the oxygen reduction reaction.*

Sample	ECSA ($m^2.g^{-1}$)	Roughness factor	ORR (0.85 V) A.g^{-1}		
			Fresh	Degraded	Change
Pd pure	33.3	3.7	7.6	7.4	2 %
Pt-Pd 0.6 h	80.8	7.9	17.4	15.2	13 %
Pt-Pd 2 h	86.8	8.4	25.9	19.9	23 %
Pt-Pd 4 h	100.6	8.5	33.5	32.9	2 %
Pt-Pd 6 h	34.7	3.4	8.9	7.3	19 %
Pt-Pd 8 h	22.6	2.2	8.8	9	2 %
Pt-Pd 17 h	69.3	6.7	11.6	11.5	1 %
Commercial Pt	84.0	7.1	18.7	16.1	14 %

After 0.6 h, the mass activity of the NPs is more than two times higher (17.4 A.g^{-1}) than the for Pd nanocubes and close to the commercial Pt nanoparticles (18.7 A.g^{-1}). From 0.6 to 4 h, the ORR activity of the particles increases further and is superior to the commercial Pt after 2 h (25.9 A.g^{-1}) and 4 h (33.5 A.g^{-1}). The galvanic replacement increases the concentration of Pt by co-deposition and replacement of Br atoms by Pt atoms increasing the number of the active sites for the ORR. The most promising particles were synthesized in 4 h, with a molar fraction for Pd of 0.7, which is favorable for the ORR. oezaslan$_pt-based_2$013, $savadogo_new_2$004, , $zhang_pdpt_2$010$TheratioPt : Pdintheoutershelloftheparticlesinfluencestheele$
$ThecatalyticperformancesfortheORRcorrelatewellwiththeECSAwithahighcatalyticactivityoftheORRinca$
$Pdalloywithdifferentcrystallineproperties(XRD, TEM).Furthermore, theshapeofnanoparticleshasalsoan$
$PdalloyNPswithdifferentsizes, wasobservedviaXRDandTEM.$

Stability of the catalyst

In addition to their catalytic performances, the particles deposited on the electrode need to be stable with no decrease of mass activity even after long times of utilization. To study the stability of the NPs, their mass activities were determined before and after 2000 CV cycles (between 0.05 V and 1.20 V with a scan range of 0.1 $V.s^{-1}$), revealing a different stability behavior (Table 4). Taking in account the experimental error ($\simeq$ 10 %), the mass activity was stable for the Pd nanocubes and the PtPd NPs that were synthesized in 4 h, 8 h, and 17 h. For the other samples, a decrease of the mass activity was observed, namely for the particles synthesized in 0.6 h (13 %), 2 h (23 %), and 6 h (19 %) as well as for the commercial Pt (14 %). The composition of the particles, as well as the atomic structure, influence significantly the catalytic performances and the stability of particles. In general, the main processes involved in the deterioration of core-shell nanoparticles are the depletion of metal atoms from the core to the particles shell, inducing an altered chemical composition and a thicker shell, as well as the coalescence and re-deposition on the metal in the surface of the particles. Furthermore, hollow nanoparticles are formed by degradation of the core-shell structure and the dissolution of Pt and Pd atoms. For the studied samples, the particles synthesized with a molar fraction of Pd of 0.70 and 0.95 show a stable catalytic activity, with a high chemical and physical stability, and are more stable than the other particles.

Comparison of the kinetic properties of the NPs for the ORR

The oxygen reduction reaction in $HClO_4$ aqueous solution at the surface of the electrode is divided in different steps following two different mechanisms, gomez-marin$_r e f l e c t i o n s_2 013, n o r s k o v_o r i g i n_2 004-1 t h e d i s s o c i a t i v e a n d t h e a s s o c i a t i v e o n e$.
The dissociative mechanism appears like the break of the O-O bond by adsorption of O atoms on chemically active site (M) on the surface of the electrode and the formation of oxides (Pt or Pd oxide) (I). The reaction of the oxide with a proton and one electron creates a hydroxide (II). The bond between Pd or Pt and OH dissociates in acid solution and water is formed.

$$O_2 + M \rightarrow O - M \quad \text{(I)}$$
$$O - M + H^+ + e^- \rightarrow OH{-}M \quad \text{(II)}$$
$$OH{-}M + H^+ + e^- \rightarrow H_2O + M \quad \text{(III)}$$

The associative mechanism includes the oxygen reduction via the formation of peroxide intermediates:

$$O_2 + M \rightarrow OO - M \quad \text{(IV)}$$
$$OO - M + H^+ + e^- \rightarrow HOO - M \quad \text{(V)}$$
$$HOO - M + H^+ + e^- \rightarrow H_2O + O - M \quad \text{(VI)}$$
$$O - M + H^+ + e^- \rightarrow HO - M \quad \text{(VII)}$$
$$HO - M + H^+ + e^- \rightarrow H_2O + M \quad \text{(VIII)}$$

The formation of H_2O_2 is also possible in step VI via the desorption of HO_2 from the surface. The occurrence of hydrogen peroxide as a stable compound in the acidic solution indicates an incomplete electron transfer.
Via Tafel and Levich analysis, the limiting step in the ORR process was investigated. The Levich analysis was executed using different rotational speeds (0, 100, 400, 900, 1600, and 2500 rpm) and the number of exchanged electrons n was calculated via the Levich equation:

$$\mathrm{i}_L = 0.602.n.F.A.C_0.D^{\frac{2}{3}}.\gamma^{-\frac{1}{6}}.\omega^{\frac{1}{2}} \quad (9)$$

where i_L ist the Levich current (or diffusion current) measured at 0.5 V, n the number of electrons, F the Faraday constant (96485 C.mol^{-1}), A the geometric area of the electrode (0.1963 cm ^{2}), C_O the concentration of the molecular oxygen in saturated solution, (1.26 $\times 10^{-6}$ mol.cm^{-3}), D the diffusion coefficient of the oxygen in the solution (1.67 $\times 10^{-6}$ mol.cm^{-2}), γ the kinetic viscosity of the electrolyte (1.009 $\times 10^{-2}$ cm^2.s^{-1}) and ω the rotational speed of the RDE (in rad.s^{-1}). The analysis revealed that the number of exchanged electrons was close to 1 (Table 5) before and after the stability test (measurements at 1600 rpm), with a diminution for the damaged samples, confirming the decrease of the catalytic activity, which was determined by the other experiments. Applying a Tafel plot, the exchange current density, j_0, an important parameter for the comparison of the catalytic properties of the NPs, was determined by the extrapolation of the experimental Tafel line to the thermodynamic potential for the oxygen reduction reaction (1.23 V) using the simplified Tafel equation:)

$$\mathrm{E} = a + b \times log(j_0) \quad (10)$$

The analysis of the Tafel plots (Figure 7, Table 5) revealed a pseudo-linear region of the curves between 0.7 and 0.9 V with two slopes, between -0.054 and 0.071 V.dec^{-1} for low current densities and between 0.107 and 0.147 V.dec^{-1} for high current densities. These slopes are in the same range as in literaturebeard$_p$*reparation*$_2$009, , *jukk*$_p$*dpt*$_2$015(0.060*V.dec*$^{-1}$ *forlowand*0.120*V.dec*$^{-1}$ *forhighcurrent*
The presence of a slope close to 0.120 V. dec^{-1} indicates that the first electron transfer is the rate determining step of the oxygen reduction reaction (with the assumption of the adsorption of O_2 according to a Langmuir isotherm). holewinski$_e$*lementary*$_2$012*Thecoverageoradsorptionofoxygencontainingsp*
*thecatalyticactivityfortheORRishigherfortheparticlessynthesizedin*0.6*hand*2*h*, *withthecurrentexchangede*

Table 5: *Evolution of the kinetic parameters determined by Tafel and Levich analysis.*

Sample	Tafel analysis		Levich analysis		
	1st Tafel slope ($V.dec^{-1}$)	2nd Tafel slope ($V.dec^{-1}$)	j_O (10^{-7} $A.cm^{-2}$)	i_L (10^{-4} A) at 0.5 V	n (1600 rpm)
Fresh samples					
Pt-Pd 0.6 h	0.060	0.119	1.8	3.68	1.28
Pt-Pd 2 h	0.069	0.130	3.6	2.33	0.81
Pt-Pd 4 h	0.066	0.125	9.6	2.64	0.92
Pt-Pd 6 h	0.054	0.112	0.3	2.37	0.82
Pt-Pd 8 h	0.064	0.112	0.8	2.56	0.89
Pt-Pd 17 h	0.059	0.132	8.7	2.68	0.93
Commercial Pt	0.071	0.139	10.0	2.52	1.24
Degraded samples					
Pt-Pd 0.6 h	0.061	0.120	1.8	2.24	0.78
Pt-Pd 2 h	0.070	0.134	3.2	2.05	0.71
Pt-Pd 4 h	0.067	0.147	7.9	2.35	0.82
Pt-Pd 6 h	0.059	0.118	0.8	2.13	0.74
Pt-Pd 8 h	0.068	0.121	1.5	2.25	0.78
Pt-Pd 17 h	0.065	0.135	9.3	2.14	0.74
Commercial Pt	0.071	0.138	8.2	2.42	0.81

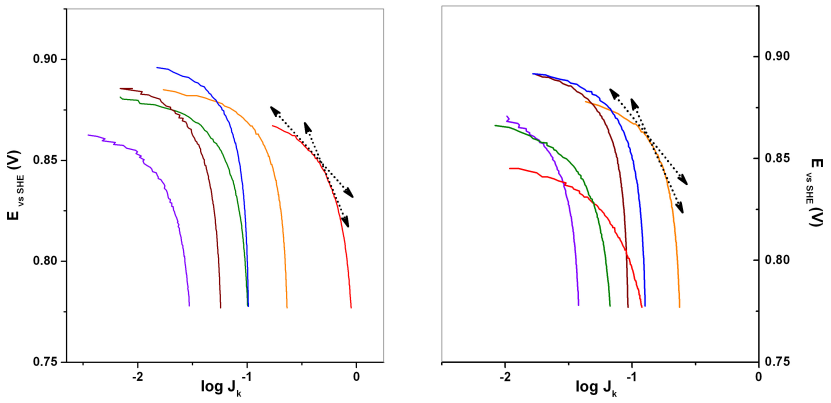

Figure 7: *Tafel diagrams plot before (left) and after (right) stability test: 0.6 h (red), 2 h (green), 4 h (orange), 6 h (violet), 8 h (brown), 17 h (blue).*

The catalytic performances of the particles could be higher with more active sites on the surface, with an easier adsorption-desorption, and with less formation of hydrogen peroxide, which poisons the ORR. For the majority of the samples, the exchange current density decreases after the stability test, indicating a degradation of the particles, leading to deteriorated catalytic properties.

Study of the mass transport phenomena by electrochemical impedance spectroscopy (EIS)

The EIS measurements were done applying a constant convection with a RDE at 1600 rpm with one aqueous $HClO_4$ (0.1 mol.L^{-1}) solution as electrolyte support ensuring negligible migration phenomena macdonald$_c$*haracterizing*$_1$998*andaconstantoxygenconcentrationattheinterfaceelectrode/electrol*

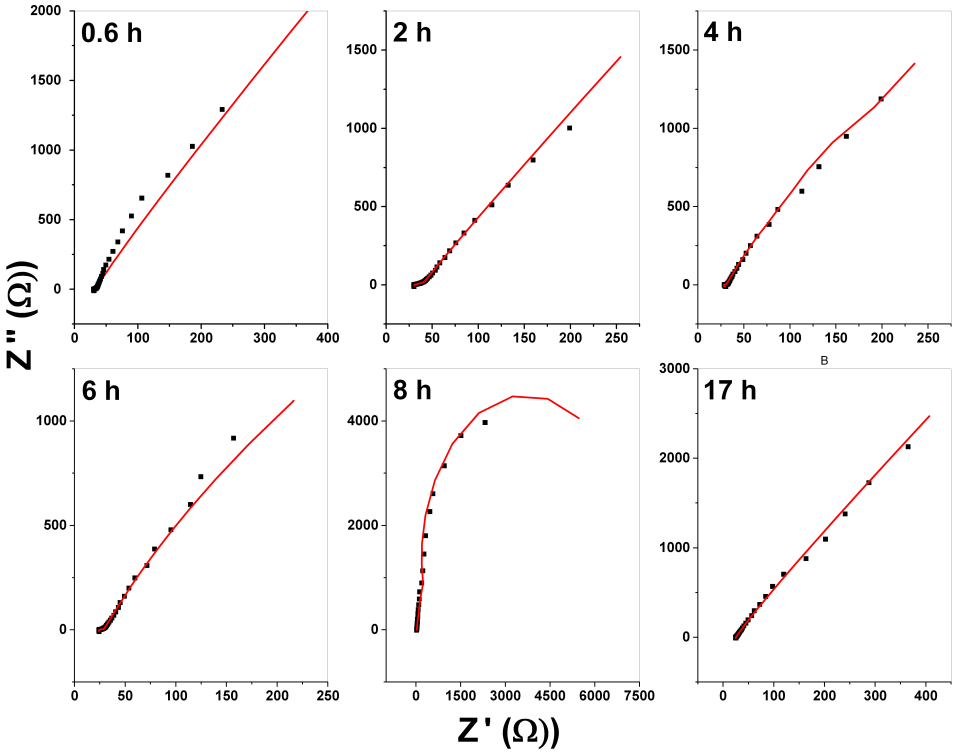

Figure 8: *Experimental (black dots) and fitted (red lines) Nyquist diagrams for the nanoparticles in function of the time of synthesis.*

The impedance was measured at a dc potential of 0.5 V, enabling a reaction that is controlled by the diffusion processes. The resulting EIS spectra, typical from diffusion controlled reaction, feature two different parts in the Nyquist plots (Figure 8).
At high frequencies, a straight line with an angle versus the x-axis that is close to 45 ° occurs for all the samples. It is followed by a degenerated arc for the 6 h and 8 h samples, while a line with an angle versus the x-axis close to 90 ° appears at low frequencies for the other samples (including pure Pt). These plots are hence similar to the theoretical diagrams of a Randles circuit macdonald$_c$*haracterizing*$_1$998, *randles*$_k$*inetics*$_1$947(*Figure*9)*withfinitediffusionwithreflectiveortransmiss*
Within the Randles model circuit, the first resistor (R_S) corresponds to the resistance of the electrolyte between the working and the counter electrode. The presence of one inductor (L),

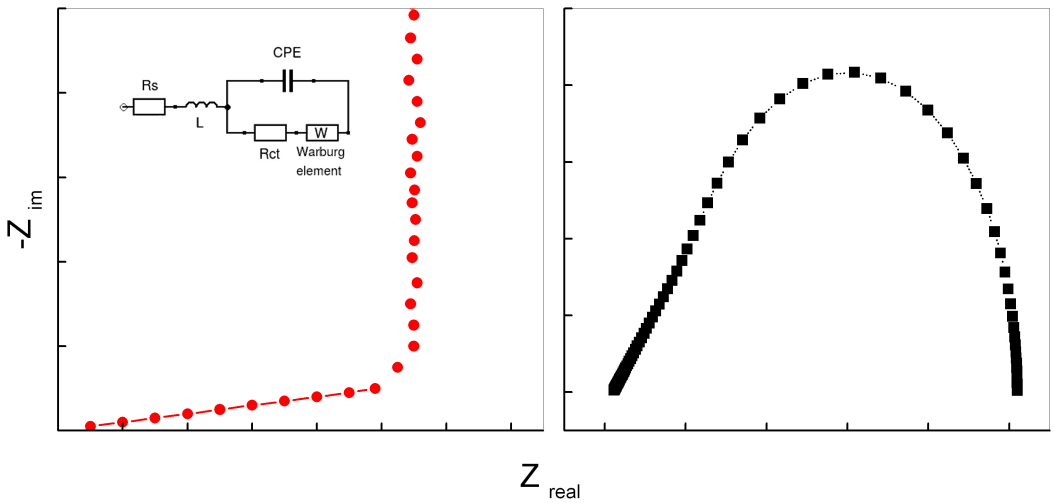

Figure 9: *Theoretical Nyquist diagrams for an finite reflective (left) and transmissive (right) diffusion, with the equivalent Randles circuit (insert)*

connected in serie with the resistor R_S traduces the experimental errors. The Faradaic processes are represented by the combination of a resistor, the charge transfer resistor (R_{CT}), which represents the resistance for charge carriers to pass the electrolyte/electrode interface, a Warburg element to model the diffusion phenomena, and a constant phase element (CPE), a non ideal capacitor, which is connected in parallel and describes the capacitance of the double layer between the electrolyte and the electrode surface. The double layer is formed by the separation of the ions and charged species accumulated at the surface of the electrode under the influence of the applied potential. The resulting capacitance is not represented by an ideal capacitor due to heterogeneities in the electrodes: rough and porous electrodes, inhomogeneous catalyst repartition on the surface of the electrode, and the Nafion layer covering the particles.
The total impedance of the system is a combination of the individual impedances of the electrical components present in the equivalent circuit:

$$Z_{TOTAL} = Z_{Rs} + Z_L + Z_{(CPE,R_{CT},W)} \tag{11}$$

with the different impedances: Z_{R_S} for the resistance of the electrolyte and $Z_{R_{CT}}$ for the charge transfer resistance, $Z_L = j\omega L$ (with the inductance L) for the inductor, $Z_{CPE} = \frac{1}{Q(j\omega)^n}$ (with $0 \leq n \leq 1$) for the CPE and Z_W for the Warburg element.

Considering a finite diffusion in the diffusion controlled region, the impedance of the Warburg element, Z_0, can be represented by the equation:

$$Z_o = \frac{R_D}{\sqrt{\frac{j\omega L_D^2}{D}}} . \tanh\left(\sqrt{\frac{j\omega L_D^2}{D}}\right) \text{ for a transmitting diffusion} \tag{12}$$

and

$$Z_o = \frac{R_D}{\sqrt{\frac{j\omega L_D^2}{D}}} . \coth\left(\sqrt{\frac{j\omega L_D^2}{D}}\right) \text{ for a reflective diffusion} \tag{13}$$

R_D is the diffusion resistance, D is the diffusion coefficient, L_D is the thickness of the diffusion layer and ω the radial frequency ($\omega = 2\pi f$).

In the case of finite diffusions, Nyquist diagrams are separated in two different regions at the diffusion frequency ω_D. Up to this, the impedance response is a pure Warburg diffusion while at lower frequencies ($\omega \rightarrow 0$), the impedance response depends on the chemical diffusing species: when a accumulation of species occurs at the surface of the electrode (x = L_D), the diffusion is reflective, with a diffusion capacitance C_D and, in case of transmitting or absorbing diffusion, the diffusing species at the surface of the electrode are directly consumed with a limiting diffusion resistance R_D, $R_D \simeq \frac{L^2}{C_D \cdot D}$. These values are dependent of the chemical system and the potential applied, without distinction between the charged species (metal, carbon support, Nafion and ionic species). The constant of diffusion for the layer of effective diffusion thickness L is defined as $\tau = \frac{L^2}{D}$.
All the Nyquist plots (Figure 8) show finite diffusion phenomena during the impedance measurements at 0.5 V. After the Warburg diffusion at high frequencies (straight line at 45 °), two different features were found: a straight line with an angle versus the x-axis close to 90 °, characteristic of a finite diffusion with reflective boundaries, corresponding to an accumulation of charges at the surface of the electrode occur for all the samples except for Pt-Pd 8 h and Pt-Pd 6 h . For these two samples, the impedance spectra are composed of a straight line at 45 ° at high frequencies and a semi-circle for the low frequencies, which is characteristic of a diffusion layer with transmissive boundary, the charges are directly consumed at the surface of the electrode. After fitting, small differences were visible between the investigated samples (Table 6).

Table 6: *Characteristics of the equivalent circuit after fitting of the impedance spectra for the different NPs.*

Sample	$\mathbf{R_S}$ (Ω)	$\mathbf{R_{CT}}$ (Ω)	**L (H)** $\times 10^{-5}$	**Q (F)** $\times 10^{-4}$	**n**	$\mathbf{R_W}$ (Ω)	$\tau_\mathbf{W}$ (s) $\times 10^{-3}$	$\mathbf{W_N}$	**L** (μ**m**)
Commercial Pt	24.6	0.16	1.4	13.9	0.85	17.9	37.8	0.47	7.95
Pt-Pd 0.6 h	30.3	1.01	1.6	1.13	0.94	11.4	7.6	0.47	3.56
Pt-Pd 2 h	30.5	0.78	1.6	5.60	0.84	49.6	42.1	0.47	8.38
Pt-Pd 4 h	28.0	0.53	1.7	0.04	0.90	11.3	12.7	0.47	4.61
Pt-Pd 6 h	23.7	0.48	1.4	0.30	0.80	14.2	13.7	0.46	4.78
Pt-Pd 8 h	34.8	0.88	1.9	3.86	0.94	73.8	10.2	0.47	4.13
Pt-Pd 17 h	31.4	0.52	1.7	1.88	0.93	18.7	4.9	0.48	2.86

The resistance of the electrolyte (R_S) is close to 30 Ω and shows only small variations. For all impedance measurements, the resistance for the charge transfer is small, around 0.5 to 1.0 Ω for the PtPd NPs and even 0.2 Ω for the pure Pt, indicating a facile charge transfer. After the fitting, R_{CT} is decreasing for the particles with one higher concentration of Pt: 1.01 Ω for the particles synthesized in 0.6 h (Pt molar fraction 4.1 %) to 0.16 Ω for the pure Pt. The particles prepared in 6 h are one exception, with the smaller resistance for the charge transfer and one Pt molar fraction of 19.5 %. This can be a result of a Pt-rich surface but in contradiction to the bad catalytic properties. The dimensionless factor of the CPE, n, is close to 1, so the parameter Q can be considered as a capacitance indicating the accumulation of charged species in the diffusion layer. The small values of Q, depending on different parameters, $wu_impedance_2015varybetween310^{-6}F(Pt-Pd4h)to1.3910^{-3}F(CommercialPt).ForallthePtPdparticles,accordingtothevaluesafterfitting,theionicaccu$ $^{-6}$ and 3 $\times 10^{-5}$ F respectively). These results are in contradiction with the ECSA: the particles synthesized in 4 h have the best ECSA but the lower capacitance. The transmitting diffusion

phenomena resorting from the impedance spectra of the particles prepared in 6 and 8 h, can reflect the low adsorption of the chemical active species (especially the oxygen) at the surface of the particles and so contribute to justify the low catalytic performances of these particles. The higher Warburg resistance, with a lower diffusion of charged species is also reducing the catalytic activity of the particles synthesized in 8 h.
For the other samples, the reflecting diffusion can traduce the adsorption of oxygen atoms and better catalytic properties but without clear link with the catalytic performances. The mass transport, represented by the Warburg diffusion resistance is dependent of the shape and chemical composition of the particles. For the particles prepared in 2 h (with the second ECSA and ORR properties) can be compensated by a higher capacitance but for the particles synthesized in 4 h, the low capacitance can not.
The diffusion of the charged species in the layer of thickness between 2.86 to 8.38 μm and with diffusion constants (τ) from 4.9 to 42.1 $\times 10^{-3}$ s is also a parameter to compare the samples. In the case of the ORR, the diffusion constant can be associated to the potential dependent adsorption of O_2, the dissociation of the O-O bond and the different chemical steps of the reaction, in function of the potential applied. The inverse of the diffusion constant, $\tau - 1$ can be assigned to the desorption rate constant of the intermediates of the ORR. At 0.5 V, the higher desorption rate is for the particles synthesized in 17 h (204.08 s^{-1}) followed by the particles synthesized in 0.6 h, 8 h, 4 h, 6 h, Pt Commercial and 2 h with significant inferior values. Compare to the particles PtPd 17 h, the diffusion layer is really thick for the pure Pt and the PtPd 2h NPs. The small values of the Warburg resistances (between 11.4 and 73.8 Ω), and the charge transfer resistances agree with structured nanoparticles possessing an high number of chemical active sites, enhancing the charge transfer and confirm the phenomena of mass transport at 0.5 V but the results of the impedance fitting are not clearly confirming the catalytic performances and the physico-chemical properties of the particles determined by TEM-EDS, XRD, EXAFS and LSV. New measurements with an higher frequency range and with an electromagnetic protection (Faraday cage) can improve the EIS characterization.

Conclusion

The palladium (core) - platinum (shell) nanoparticles were synthesized by galvanic replacement and studied after different times of synthesis to establish relationships between the physical properties, the chemical composition and the catalytic properties regarding the oxygen reduction reaction, a crucial reaction in fuel cells. TEM measurements revealed the evolution of the shape of the particles, from *fcc*-cubic pure palladium to cubic-concave core-shell bimetallic nanoparticles. The chemical composition of the particles varies, with an increasing amount of platinum until 4 h of synthesis (Pt molar fraction 0.3), and a subsequent decrease until 8 h, followed by a final increase up to 17h. However, future experiments that offer a higher precision (ICP-MS) are necessary. The formation of a platinum-palladium alloy within the outer shell of the particles and a modification of the structure of the nanoparticles was revealed by EXAFS studies and by XRD measurements, respectively. Further XPS and *in-situ* XPS experiments would be helpful to complete the characterization of the particles. The determination of the electrochemically active surface area and of the activities for the oxygen reduction reaction by cyclic voltammetry permitted to compare the catalytic performances and stabilities of the nanoparticles. Expectedly, the addition of platinum with the formation of an alloy in the shell of the particles influences the catalytic activity and stability. After 0.6 h, particles with a small amount of platinum (molar fraction of 0.05) and an activity and stability close to a pure commercial platinum catalyst are obtained. After 2 h, the catalyst shows a superior catalytic

activity compared to the pure platinum and the best performance is achieved for the particles synthesized within 4 h, with a stable catalytic activity that is two times higher than for pure platinum and a lower amount of the expensive metal (Pt molar fraction of 0.7).

Acknowledgements

We thank all the research group working at the Rossendorf Beamline BM20 A (ESRF, Grenoble, France), Dr Stephanie Höppener for TEM and EDS mapping, Dr Sindy Fuhrmann for the access to the XRD and her help for the Rietvield analysis, Dr Igor Perevyazko for his help and the access to an high speed centrifugation machine. Thank also to all the technicians of the workshop of the university for the participation in the fabrication and test of the experimental cells. This study was accomplished with the financial help of the Carl Zeiss Foundation (Germany).